NACA RM A57C25

NATIONAL ADVISORY COMMITTEE FOR AERONAUTICS

RESEARCH MEMORANDUM

INVESTIGATION OF BOUNDARY-LAYER TRANSITION

ON FLAT-FACED BODIES OF REVOLUTION

AT HIGH SUPERSONIC SPEEDS

By Thomas N. Canning and Simon C. Sommer

SUMMARY

The boundary-layer transition characteristics of bodies of revolution having flat and nearly flat faces were investigated experimentally. The models, right circular cylinders and similar shapes, were tested at Mach numbers from 2.5 to 9. The Reynolds numbers based on free-stream conditions and model diameter ranged from 2.5×10^6 to 9.1×10^6. Shadowgraphs indicated that the boundary layer remained laminar on the front faces and was turbulent only on the sides. The Reynolds numbers (based on local air properties integrated over the distance from the stagnation point) were always below 1 million on the faces. The transition Reynolds numbers, when considered on the basis of this integrated Reynolds number, are consistent with earlier results for round-nosed bodies of low fineness ratio.

The tests also yielded information on the total drag coefficients and static longitudinal stability of the models. The drag coefficients approached the pitot-pressure coefficient and all bodies were statically stable in pitch.

INTRODUCTION

The problem of reducing the heat input to missiles entering the earth's atmosphere at extremely high velocity may be attacked in several ways. Two approaches which involve no mechanical complication of the missile are: (a) design the body to have large pressure drag and small wetted area, and (b) provide a shape which will have a low total heat-transfer coefficient. The first approach is treated by Allen and Eggers in reference 1. The preservation of extensive laminar flow is one di   t method of using the second approach. Reference 2 reports the results several attempts to use the second approach, maintenance of laminar

boundary-layer flow, on shapes which satisfied the requirements of the first approach. The results of reference 2 indicate that only small portions of the boundary-layer flow would be laminar at full-scale Reynolds numbers for the configurations tested, principally round-nosed cones and hemispheres. The areas on which turbulent flow was present were also areas where the static pressure and flow velocities were high. The heat transfer to such areas is expected to be extreme.

In reference 2 it is observed that the Reynolds numbers of transition, based on conditions just outside the boundary layer, appeared to range around 1 million regardless of moderate changes in model shape and roughness. In reference 3 it is further observed that the Reynolds numbers based on local air properties outside the boundary layer can, for a given free-stream Reynolds number, be reduced by blunting. The above factors lead logically to shapes having flat faces normal to the stream to give minimum local Reynolds numbers, although this configuration was not first considered on such a logical basis. Rather, some shadowgraphs of nylon slugs (right circular cylinders), used in obtaining interior ballistic data, showed laminar flow over the entire front face, laminar separation at the corner between face and sides, and transition to turbulent flow at the reattachment point. With this promising first result, laminar flow on the front face, the present exploratory investigation was started.

The present paper describes results of a brief experimental program conducted to verify this observation. In addition to observations of boundary-layer transition, the tests yielded information on static stability and drag.

Heat-transfer data for bodies much like those used in the present tests, reference 4, showed low values of heat transfer over the entire front face of all flat-faced models tested. Low heating rates were noted on the sides of several of these models as well. Tests of several bodies in a 4000° F supersonic jet, reference 5, showed that flat-faced models survived far longer under severe test conditions than did any other shape tried.

NOTATION

A   frontal area, sq ft

A_f area of model face inside the rounding at corner between face and sides

C_D drag coefficient, $\dfrac{D}{q_\infty A}$ and $\dfrac{D}{q_\infty A_f}$

C_{m_α} pitching-moment-curve slope, $\dfrac{1}{q_\infty A d} \dfrac{dM}{d\alpha}$, per radian

D   drag, lb

d   maximum diameter, ft

M   pitching moment about model center of volume, ft-lb

m   mass, slugs

M_∞ free-stream Mach number

q_∞ free-stream dynamic pressure, lb/sq ft

R_∞ Reynolds number based on model diameter and free-stream
             conditions

R_{edge} Reynolds number based on averaged conditions outside the boundary
             layer from the stagnation point to the edge of the flat face,

$$\int_{SP}^{edge} \frac{\rho_1 u_1}{\mu_1}\, dS$$

R_δ, R_θ Reynolds number based on local conditions and boundary-layer
             dimensions

S   distance along a surface streamline from the stagnation point,
             ft

SP   stagnation point

u_∞ velocity of free stream, ft/sec

u_1 local velocity outside boundary layer, ft/sec

α angle of attack, radians

δ boundary-layer thickness, ft

θ boundary-layer momentum thickness, ft

ρ_1 air density just outside the boundary layer, slugs/cu ft

ρ_∞ air density of free stream, slugs/cu ft

μ_1 coefficient of viscosity of air just outside boundary layer,
             lb sec/sq ft

μ_∞ coefficient of viscosity of free-stream air, lb sec/sq ft

APPARATUS AND TESTS

The tests were conducted in the Ames supersonic free-flight wind tunnel and the supersonic free-flight underground range. The former is a 24-foot-long ballistic range with nine shadowgraph stations inside a variable-pressure, supersonic, blowdown wind tunnel. The latter is a 67-foot-long ballistic range with seven shadowgraph stations. At test Mach numbers below 5.0 the models were fired from a 1-3/4-inch smooth-bore gun through still air either in the wind tunnel or in the underground range. The model temperature is approximately equal to the free-stream static temperature for these tests. At Mach numbers above 5.0 the same gun was used, and the wind tunnel was operated at a Mach number of 3.0. This resulted in a model temperature about 2.8 times the free-stream temperature. Reference 6 describes the features of the wind tunnel in detail. The modifications to the equipment mentioned in a footnote in reference 6 have been completed. The four shadowgraph stations spaced 5 feet apart have been replaced with nine shadowgraph stations 3 feet apart. In addition, improved design and construction techniques resulted in a much more uniform air stream.

MODELS

The models are all sketched in figure 1. The basic shape is a right circular cylinder, and small deviations from this shape were tested. All of these models, except models A and C, were made of 7075-T6 aluminum. Models A and C were made of nylon. No special care was taken in polishing the surfaces of most models. The machinist removed tool marks using successively finer abrasive papers, ending with No. 600 grit. This surface had many circumferential scratches, 15 to 60 microinches deep.

One model was polished with extreme care to obtain what is termed a "type III" surface in reference 2. This surface was produced by eliminating all machine marks with coarse abrasive paper, polishing with successively finer grades of abrasive paper, through 4/0, and then polishing with successive grades of aluminum-oxide abrasive. The finest grade used was 20-microinch grit. The resulting surface has few scratches but has many small pits and bumps, about 5 to 10 microinches amplitude. In the section on results and discussion, the model thus treated will be noted.

DATA REDUCTION

Drag and Static Stability

The drag coefficients of the models tested were calculated from the axial deceleration; the pitching-moment-curve slope about the models'

centers of volume were calculated from the pitching frequencies. These data-reduction techniques are detailed in reference 6. The drag coefficients and moment-curve slopes are believed to contain maximum errors of ±3 percent.

Boundary-Layer Transition

Each shadowgraph picture was studied in the manner described in reference 2 for the occurrence of transition from laminar to turbulent boundary-layer flow. The characteristics of the shadowgraphs used to establish the presence of turbulence are illustrated in the accompanying sketch and are discussed below:
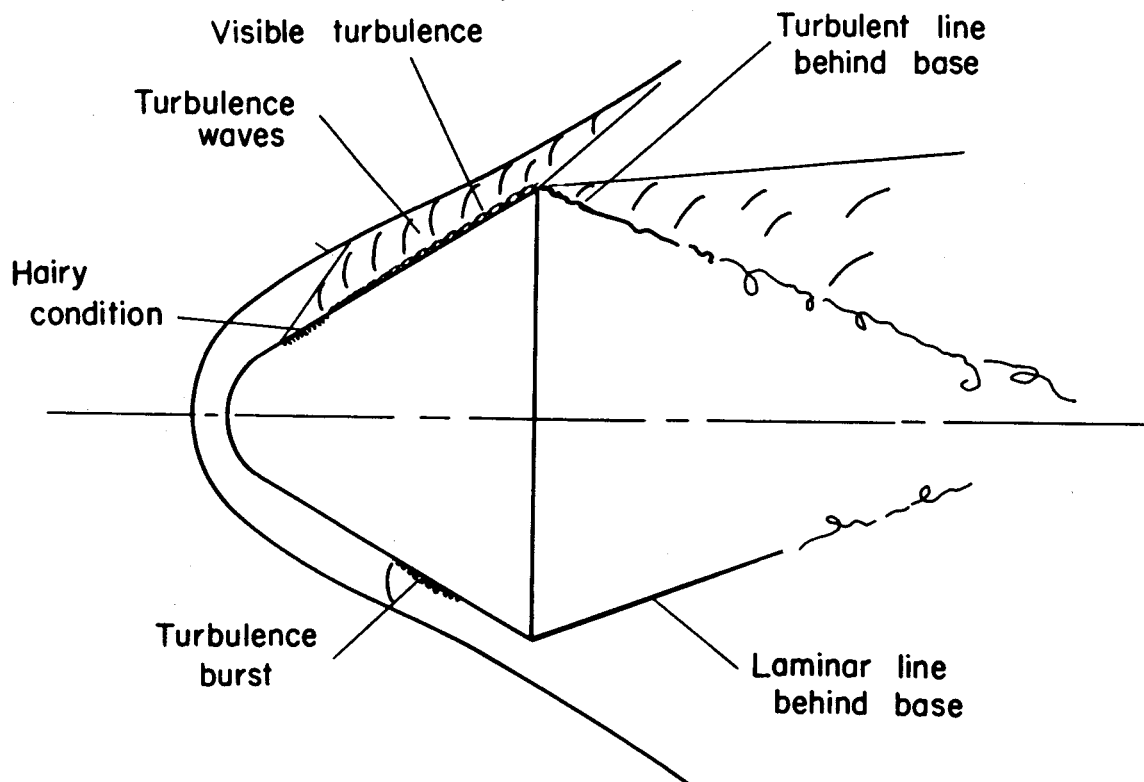
(a) In some cases the refraction of light passing through an eddy of turbulence was sufficient to produce an easily visible image. In the present tests this type of image was seen only on the sides of models and in the wakes, never on the front faces.

(b) Where the boundary layer was exceedingly thin, the front faces for example, the refraction did not produce clear images such as described above but did project small filaments of light onto the portion of the film shaded by the model. This gave a hairy appearance to the model shadow. This hairiness was sometimes visible outside the model shadow as well.

(c) A region of supersonic flow outside a turbulent boundary layer contains many weak, irregular shock waves. There usually appear to be two families of waves; one family, which lies along Mach lines, appears to result from body-fixed disturbances, and the other family, which is inclined more steeply to the flow than Mach lines, appears to result from moving disturbances, individual eddies, or groups of eddies passing along the body. The body-fixed disturbances probably emanate from surface roughness, the effect of which is accentuated by the extreme thinness of the laminar sublayer.

(d) The condition of the boundary layer on the model can frequently be deduced from the image of the wake. An initially laminar layer gives a thin, smooth, steady line which may extend as far as a model diameter behind the base. An all-turbulent wake, on the other hand, produces a poorly defined, noticeably wavy line which washes out rapidly.

Caution is necessary in interpreting all of the above evidences of turbulence, particularly the wake-flow indications. For instance, it is entirely possible for turbulent flow on the face of the present models to undergo sufficient acceleration around the corner to become essentially laminar, as noted by Sternberg (ref. 7). Thus an observation of laminar flow at one point on the body does not mean that the flow upstream is necessarily all laminar.

In order to test the usefulness of shadowgraphs for detecting turbulence on the front faces, a model (model E, fig. 1), which had No. 60 Carborundum grit on its face, was tested (see fig. 2(a)). The hairy condition described above was very clearly developed. On a subsequent test of model E with a smooth face, a burst of turbulence was noted, in one station only (leader in fig. 2(b)). These observations showed that turbulence on the model face would be apparent in the shadowgraphs.

The density gradients in the flow fields about the models produced optical distortion in all the shadowgraphs. The distortion of the model images was optical only, since the models were not deformed.

RESULTS AND DISCUSSION

Boundary-Layer Transition

No particular difficulty was encountered in obtaining fully laminar flow over the entire front face of the configurations tested at nominal Mach numbers of 4 and 9 and free-stream Reynolds numbers of 4 million based on diameter. The same appears true of one test of a highly polished model at a Mach number of 3.2 and free-stream Reynolds number of 9 million based on model diameter. This latter test will be discussed in some detail subsequently. Transition to turbulent flow usually occurred along

the sides of the models, although in some cases the flow was laminar into the wake. Selected shadowgraphs from the tests are presented in figures 3 through 8 to illustrate as well as possible, with the loss of detail suffered in reproduction, the important features of the flow. Each of these figures is described below to offset some of the loss of photographic clarity.

Figures 3(a) and 3(b) were obtained during the interior ballistics tests mentioned in the introduction by use of a simple right circular cylinder, model A. The separation of the boundary layer from the edge of the front face is easily seen as are the flow reattachment and turbulent eddies along the sides. No evidence of turbulence was noted on the front face. The shadowgraph of a somewhat shorter circular cylinder, model B, flying at a higher Mach number, figure 3(c), is made difficult to analyze by the background "hash" from the wind-tunnel boundary layer, but the original negatives from this test showed good evidence that the flow was always laminar on the face. Turbulence occurred intermittently on the sides.

Model C, the 170° included-angle cone-cylinder, figure 4, shows much the same boundary-layer flow as noted for the flat-faced cylinder. The effect of slight convex curvature on the front face and 5° of flare on the sides was investigated with model D (see fig. 5). The original negatives showed transition to be either on the sides of the model or behind the base. The only difference between this result and that from model B (right circular cylinder) was that the size of the separated region was smaller in the case of model D.

Model E differed from model D by being boattailed instead of flared. The flight of model E, figure 6, was admirably suited to show the separation of the laminar layer from the front-face edge. These two shadowgraphs were made during one flight. The flow has more than one possible configuration and was observed to alternate between laminar reattachment on the side, figure 6(a), and fully separated flow, figure 6(b). When the flow failed to reattach, transition occurred at or just behind the sharp edge.

Model F, which was like model D except for a rounded rather than sharp edge, shows no separation region, figure 7, and transition appears to have taken place near the model base at the lower Mach number and well behind the base at $M_\infty = 8.7$, figure 7(c). The steady wavelets from one side of the model of figure 7(a) were caused by surface roughness. A smooth, gradual compression may be seen to occur along the sides of this model, which contrasts strongly with the sudden compression at the flow reattachment point of the sharp-edged models discussed above.

Figure 8 was obtained from the test of a highly polished model (model F) fired through still air at high pressure in the wind tunnel. The Mach number was 3.2 and the free-stream Reynolds number was 9.1 million

based on model diameter. What may have been transition was noted at the
beginning of the rounded corner. The hairy image, in this case, was
visible outside the body shadow. In this picture there may be seen a
background graininess which, when distorted by the bow shock wave, looked
somewhat like the hairy image typical of turbulence; although there is
some small doubt on this point, transition probably occurred early on the
sides of this model.

In order to make the maximum use of this information, it is desirable
to formulate a criterion which will make comparison with other boundary-
layer transition observations feasible. More important, however, the
criterion should make it possible to apply test data to full-scale flight
at Mach numbers and Reynolds numbers higher than those obtained in the
present tests. Because present knowledge of the transition process and
the events leading up to transition is insufficient, such a selection
must be made empirically.

One possible criterion which is readily calculated is, of course,
the local transition Reynolds number based on local flow properties just
outside the boundary layer at the transition point, and length of boundary-
layer run from the stagnation point. However, comparison of the present
results with those of reference 2 shows that the local transition Reynolds
numbers of the present tests are greater by factors of 2 to 3 than those
of reference 2. This is clearly inconsistent with the principle that a
transition criterion computed so as to include the effect of changes in
body shape should be a constant.

In the tests of reference 2, the region of large variations in flow
properties was confined to about 25 percent of the length from the stag-
nation point to the transition point because the nose radii were relatively
small (1/3 of base radius for one model). In the present tests, where
the bluntness was much greater, the flow conditions varied continually
from the stagnation point to the face edge. In order to take account of
this difference in shape the Reynolds number was calculated as an integral
of the local air conditions along the streamlines, instead of using local
conditions at the transition point.

The transition Reynolds numbers of reference 2 would be about the
same for both methods of calculation, and the present results are made
consistent with them.

The Reynolds numbers were calculated at the face edge using

$$R_{edge} = \int_{SP}^{edge} \frac{\rho_1 u_1}{\mu_1} \, dS$$

The conditions assumed for these calculations were: (a) the air was
behaving like a perfect gas and (b) the pressure distribution was identical

to that measured by Oliver on a flat-faced body in reference 8, ignoring the slight dip in pressure noted at the stagnation point in Oliver's data.

The results of these calculations are presented in figure 9 in the form of the integrated Reynolds number at the face edge divided by free-stream Reynolds number based on diameter as a function of free-stream Mach number. Note that this ratio is always less than 0.1 at Mach numbers above 4. Also included in this figure is the same ratio estimated assuming equilibrium dissociation and vibration behind the normal shock wave and no relaxation downstream. These latter calculations were based on references 9 and 10 and are highly approximate. It is believed that the ratios are conservatively high because it was assumed no recombination occurred as the air accelerated.

The maximum integrated Reynolds number on the model face in the present tests was in the neighborhood of 0.7 million. It is important to note that the Reynolds numbers quoted are for flat faces whereas most of the models used had convex faces. Therefore, the maximum Reynolds number quoted is doubtless too low. No pressure-distribution data are available for these convex shapes to aid in estimating the error involved.

The variation with Mach number of the Reynolds number at the face edge for three flat-faced missiles 1 foot in diameter entering the atmosphere at high speed is plotted in figure 10. These examples are the same as those used in reference 2. If differences in heat transfer and the effects of dissociation do not invalidate extrapolation of the present results to higher speeds, it appears possible to have laminar flow over the face of a missile 4 feet in diameter until the Mach number has been reduced below 12, provided the value of $C_D A/m$ is kept above 0.2 square foot per slug.

The flat face is clearly not the ultimate shape for reducing local Reynolds numbers. The ultimate is probably a deep (open side forward) cup. The pressure in the cup is constant so that velocities are zero on the inside surfaces and hence we have true stagnation conditions. This shape is probably of interest only as a limit, but the possibility of dishing the face in slightly may lead to further reduction in Reynolds number per foot. It may, in fact, give such low velocities that no danger exists of having turbulent boundary layer on the face. The concomitant dangers of increased heat flow at the edges and possible flow instability in the dish (and loss of static longitudinal stability) must be considered before such shapes are seriously proposed. Heat-transfer measurements on two such bodies, reference 4, indicated low heat-transfer rates in the dished area and around the rounded corners as well.

The low values of local test Reynolds number can also be thought of in terms of boundary-layer-stability theory, where normally the bounda·· layer Reynolds numbers, R_δ and R_θ, are used to define the region where

Tollmein-Schlicting waves may be amplified. These Reynolds numbers were
estimated, using the results for spheres given in reference 2, for the
highest free-stream Reynolds number of the present investigation. The
value of R_δ at the model edge was about 1200 and an assumed ratio
of $\delta/\theta = 6$ gave $R_\theta = 200$. These values were low enough so that wave
amplification probably did not occur. In reference 2, however, one case
was reported where transition occurred within 7° from the stagnation
point of a hemisphere, at which point R_θ was much smaller than at the
corner of the present models. Therefore, it must be concluded that some
other disturbing factor, perhaps roughness, was influencing transition in
the case of the hemisphere test. Calculations indicate that the boundary-
layer thickness at the stagnation point of the present models is about
4 times that on the hemisphere, and about 10 times that on the round-
nosed 60° cone of reference 2. This difference probably reduced the
sensitivity to roughness in the present tests in that the ratio of
roughness height to boundary-layer thickness is reduced.

The flow conditions at the corner and along the sides of the models
are discussed below. For those models with sharp edges the flow separated,
see figures 3 through 6, and the introduction of very slight rounding
appeared to suppress separation completely, see figures 7 and 8. The
relative merits of rounded versus sharp edges cannot be settled by the
tests reported here; rather, the effect this change in shape has on local
and total heat-transfer rates will probably answer the question. The
theory of reference 11 indicates, for instance, that the surface heating
through a separated laminar layer is about one half that for attached
laminar flow. However, when the detached flow from the sharp edge
reattaches to the side, a sharp compression results and transition to
turbulent flow usually ensues (figs. 2 through 6). In these regions
where turbulent flow is most likely to occur the static pressure, and
hence density, is relatively low so that the heat transfer may still be
tolerable.

One additional feature of the flow field noted in some of the shadow-
graphs was a series of lines parallel to the model face in the region
between the face and the bow wave (leader in fig. 3(c)). It was suggested
that these were waves from longitudinal vibration of the model. If these
were compression waves emanating from near the surface, traveling at the
local speed of sound, the calculated frequency is around 3 megacycles.
This frequency is about 30 times higher than the natural frequency of an
elastic wave traveling through the model parallel to its axis; this
essentially rules out elastic waves as the cause. These same lines have
been seen in spark shadowgraphs of sting-mounted blunt bodies taken in
the Ames 8- by 7-foot supersonic tunnel and the 6-inch heat-transfer
tunnel, and are believed to be either pressure pulses oscillating in the
subsonic flow region, or Goërtler vortices lying along streamlines.

Drag

The drag data obtained in these tests are presented in figure 11(a).
These coefficients are based on model frontal area. In figure 11(b)
these same data are plotted using the face area for reference. The pres-
sure drag measured by Oliver and an unpublished result from the Ames
6- by 6-inch heat-transfer tunnel for a flat-faced body at a free-stream
Reynolds number of 0.6×10^6 are noted in this figure, as is the variation
of pitot pressure coefficient with Mach number. The agreement between
the pitot pressure coefficient and the total drag coefficient based on
the face area suggests the ease with which total drag may be estimated.

The high values of C_D can be a boon to the missile designer who
wishes to reduce the over-all body size without affecting the param-
eter $C_D A/m$ discussed in reference 1. Since C_D is more than 50 percent
larger than for a sphere, the frontal area may be reduced by more than
33 percent, and as a direct result of reduced size, some saving in struc-
tural weight may be possible. This comparison is even more favorable to
the right circular cylinder when the round-nosed cone (ref. 2) is the
alternative, since the ratio of drag coefficients approaches 3.

Static Longitudinal Stability

The values of C_{m_α}, pitching-moment-curve slope, about the models'
centers of volume, including the stud in the model base, are plotted in
figure 12. Since normal-force-curve slope is not known, it is not possible
to transfer the reference axes. These values are based on frontal area
and diameter, as references. Little can be deduced from these data except
that all bodies were stable and the small changes in shape did not produce
important changes in static stability.

It is of interest to note that Newtonian impact theory does not
predict C_{m_α} correctly for shapes of this sort. In the case of the
right circular cylinder, the predicted value of C_{m_α} would be zero at
all angles of attack. This is clearly not so.

CONCLUDING REMARKS

Tests conducted in the Ames supersonic free-flight wind tunnel have
shown that laminar boundary-layer flow may be maintained over the faces
of bodies resembling right circular cylinders at Reynolds numbers
of 9 million at a Mach number of 3.2, and 4 million at a Mach number of 9.

In the former case transition may have occurred at the edge of the face; in the latter case the boundary layer was frequently laminar over the entire surface and into the wake.

The drag of the bodies was very large. Values of total drag coefficient approaching the pitot-pressure coefficient were measured.

All the bodies tested exhibited stable static longitudinal stability about their centers of volume. No theory known to the authors accurately estimates static stability for this type of body.

Ames Aeronautical Laboratory
      National Advisory Committee for Aeronautics
            Moffett Field, Calif., Mar. 25, 1957

REFERENCES

1. Allen, H. Julian, and Eggers, A. J., Jr.: A Study of the Motion and Aerodynamic Heating of Missiles Entering the Earth's Atmosphere at High Supersonic Speeds. NACA RM A53D28, 1953.

2. Seiff, Alvin, Sommer, Simon C., and Canning, Thomas N.: Some Experiments at High Supersonic Speeds on the Aerodynamic and Boundary-Layer Transition Characteristics of High-Drag Bodies of Revolution. NACA RM A56I05, 1957.

3. Moeckel, W. E.: Some Effects of Bluntness on Boundary-Layer Transition and Heat Transfer at High Supersonic Speeds. NACA TN 3653, 1956.

4. Carter, Howard S., and Bressette, Walter E.: Heat Transfer and Pressure Distribution on Six Blunt Noses at a Mach Number of 2. NACA RM L57C18, 1957.

5. Purser, Paul E., and Hopko, Russell N.: Exploratory Materials and Missile-Nose-Shape Tests in a 4000° F Supersonic Air Jet. NACA RM L56J09, 1956.

6. Seiff, Alvin: A Free-Flight Wind Tunnel for Aerodynamic Testing at Hypersonic Speeds. NACA Rep. 1222, 1955.

7. Sternberg, Joseph: The Transition from a Turbulent to a Laminar Boundary Layer. B.R.L. Rep. No. 906, Aberdeen Proving Ground, Md., May 1954.

8. Oliver, Robert E.: An Experimental Investigation of Flow Over Simple Blunt Bodies at a Nominal Mach Number of 5.8. GALCIT Memo. No. 26, June 1955.

9. Gilmore, F. R.: Equilibrium Composition and Thermodynamic Properties of Air to 24,000° K. RM-1543, Rand Corp., Aug. 1955.

10. Mayer, Joseph Edward, and Mayer, Maria Goeppert: Statistical Mechanics. John Wiley and Sons, Inc., 1940.

11. Chapman, Dean R., Kuehn, Donald M., and Larson, Howard K.: Preliminary Report on a Study of Separated Flows in Supersonic and Subsonic Streams. NACA RM A55L14, 1956.
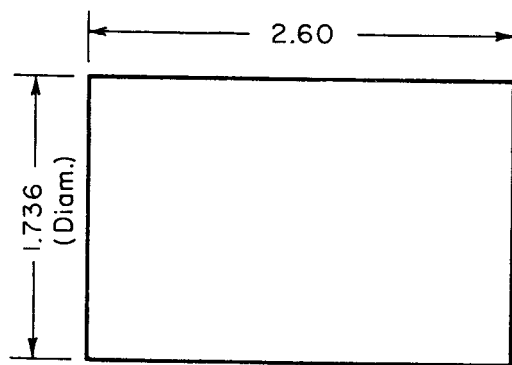
(a) Model A

All dimensions
in inches
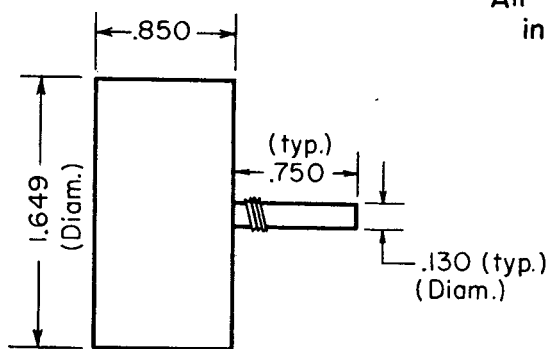
(b) Model B
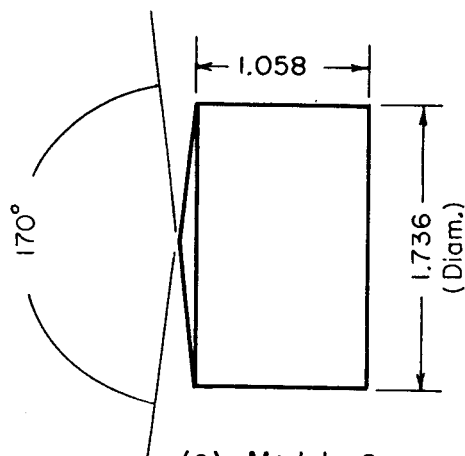
(c) Model C

Figure 1.- Models.
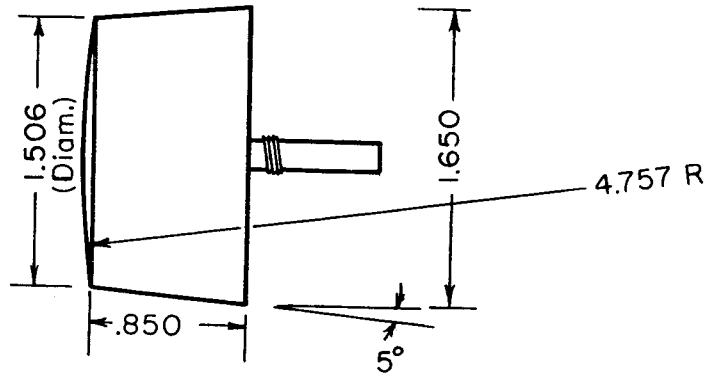
(d) Model D
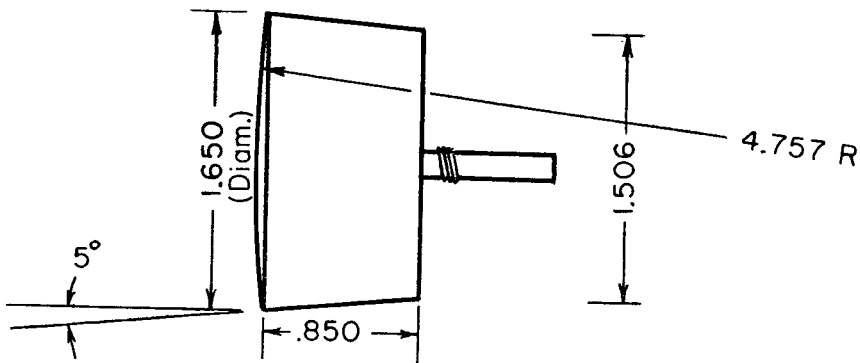
(e) Model E
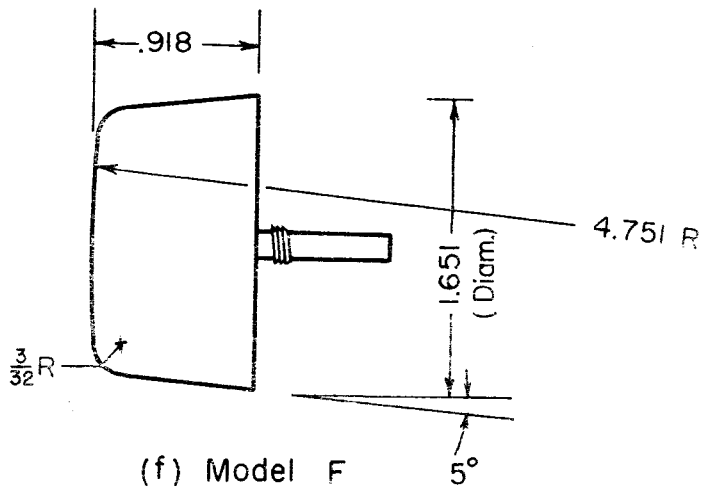
(f) Model F

Figure 1.- Concluded.
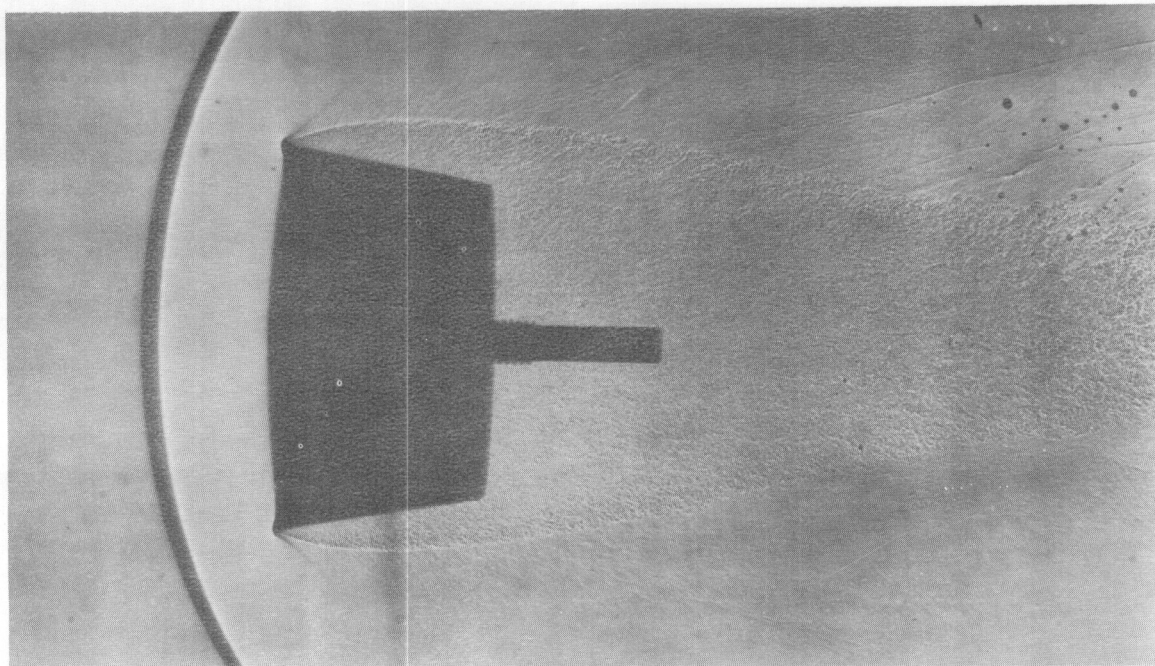
(a) Face roughened with No. 60 Carborundum grit; $M_\infty = 2.3$, $R_\infty = 2.2 \times 10^6$.
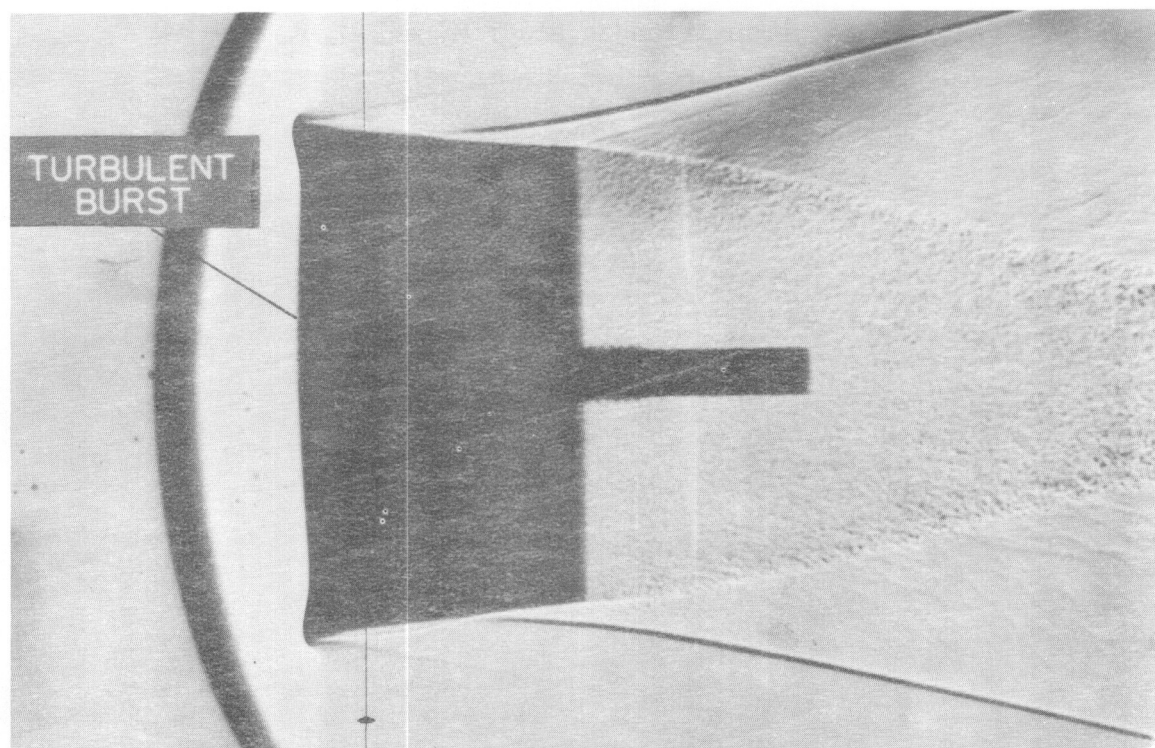
(b) Turbulent burst on smooth face; $M_\infty = 2.8$, $R_\infty = 2.8 \times 10^6$.

Figure 2.- Turbulent flow on face of model E.
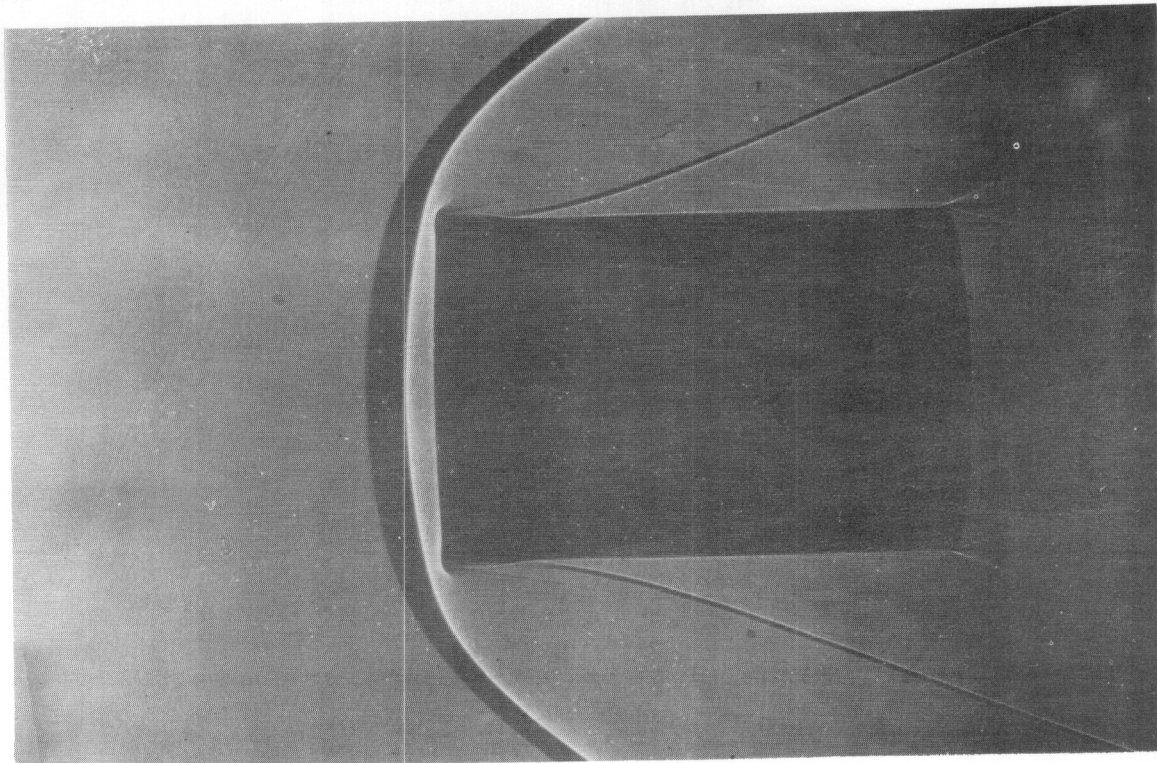
(a) Model A, transition on side; $M_\infty = 3.8$, $R_\infty = 4.0 \times 10^6$.
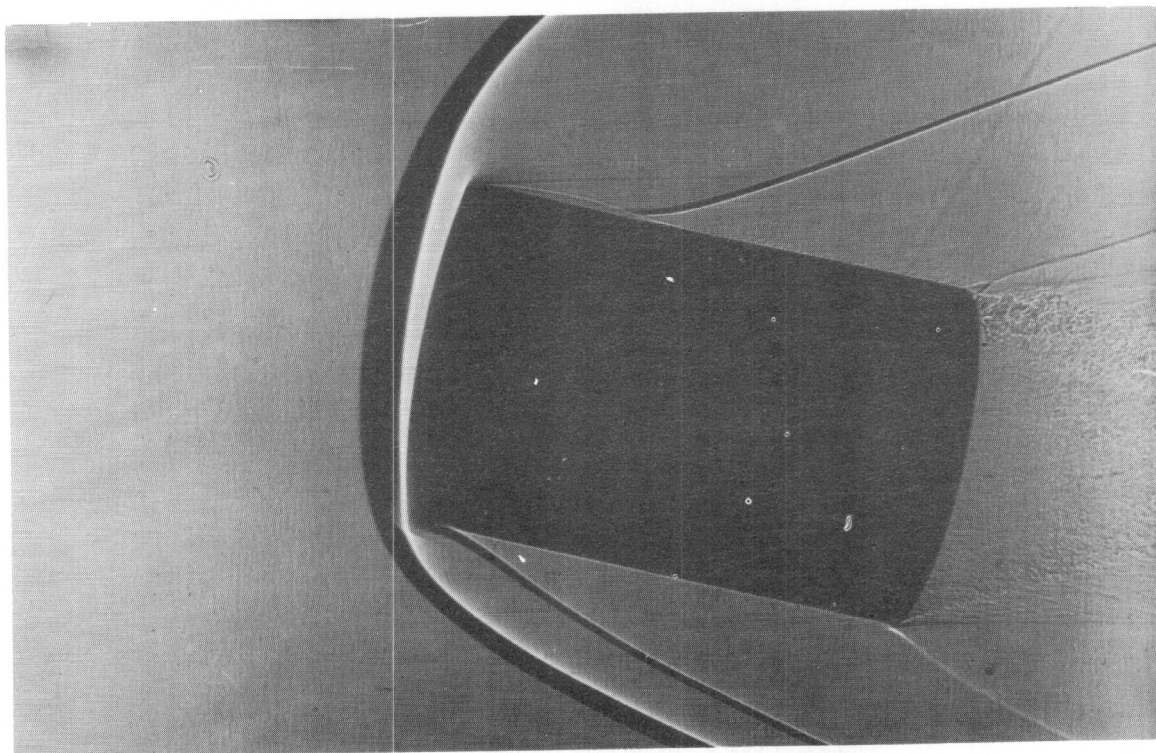
(b) Model A, transition on side; $M_\infty = 3.8$, $R_\infty = 4.0 \times 10^6$.

Figure 3.- Laminar flow on face of circular cylinders.
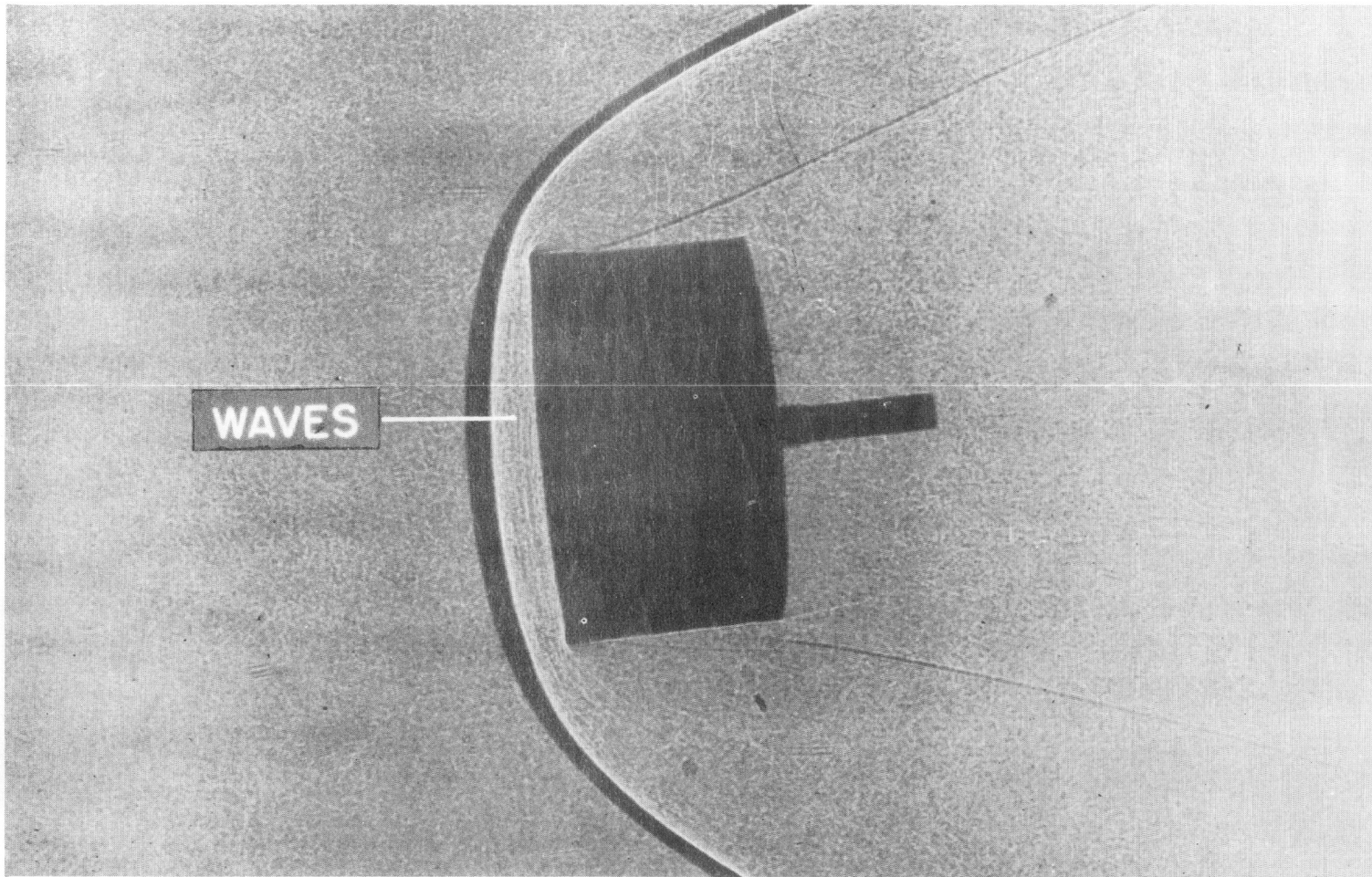
(c) Model B, transition in wake; $M_\infty = 8.8$, $R_\infty = 4.8\times10^6$.

Figure 3.- Concluded.
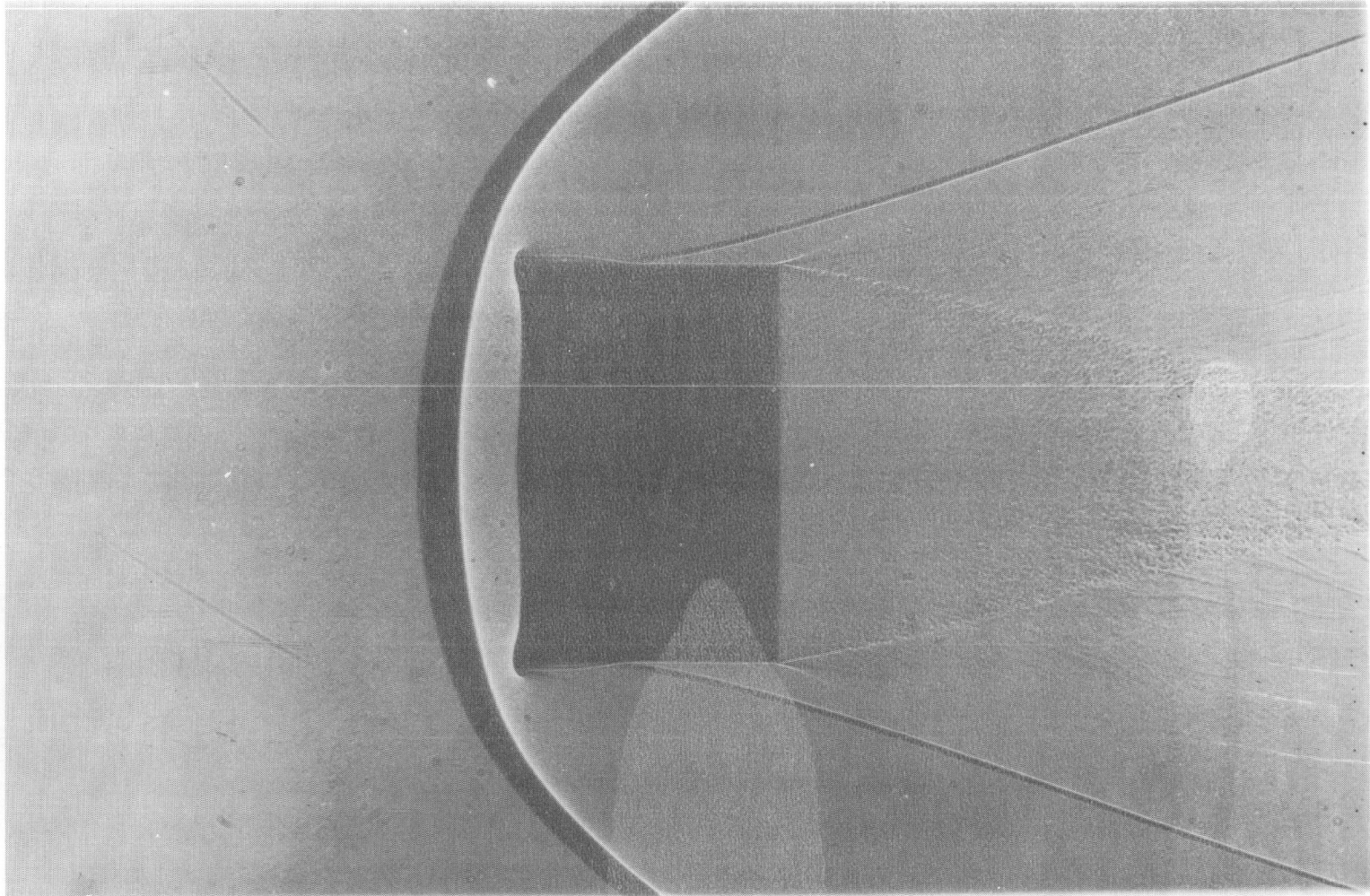
Figure 4.- Laminar flow on face of model C; $M_\infty = 3.5$, $R_\infty = 3.3\times10^6$.
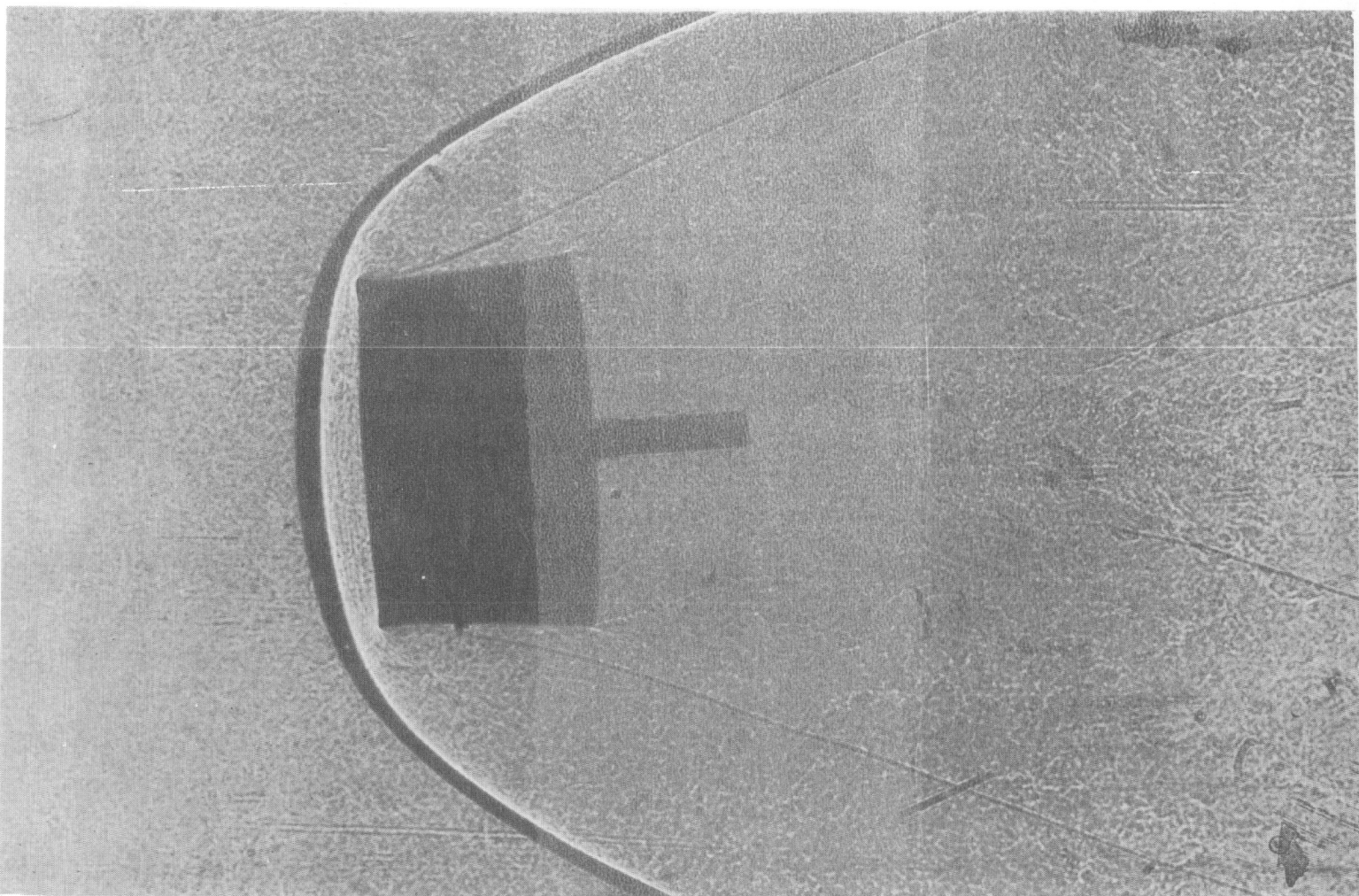
Figure 5.- Laminar flow on face of Model D; $M_\infty = 8.8$, $R_\infty = 4.7 \times 10^6$.
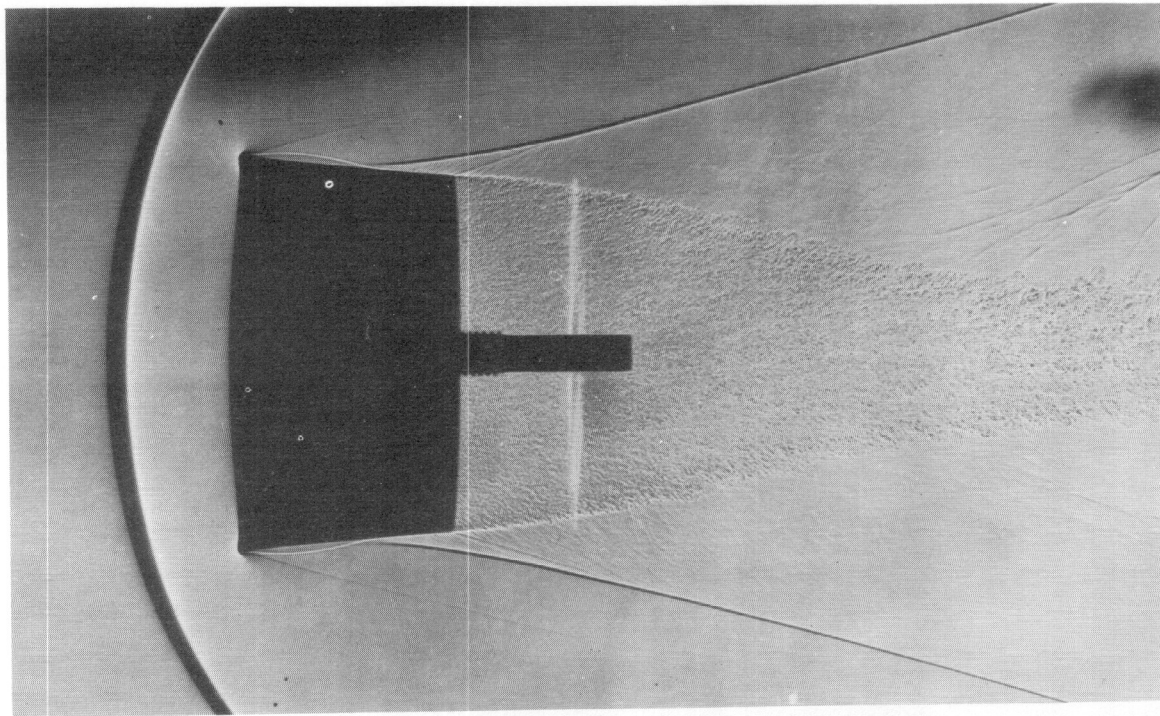
(a) Flow reattaches before transition.
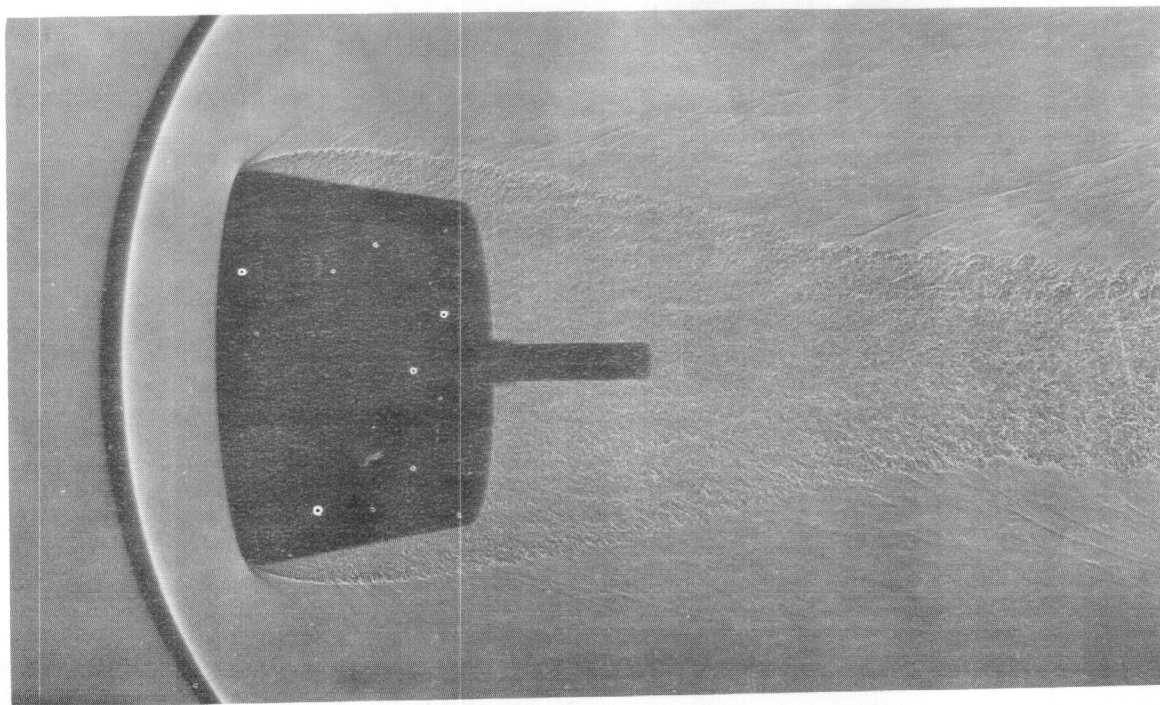
(b) Flow fails to reattach.

Figure 6.- Laminar flow on face of model E; $M_\infty = 2.5$, $R_\infty = 2.5 \times 10^6$.
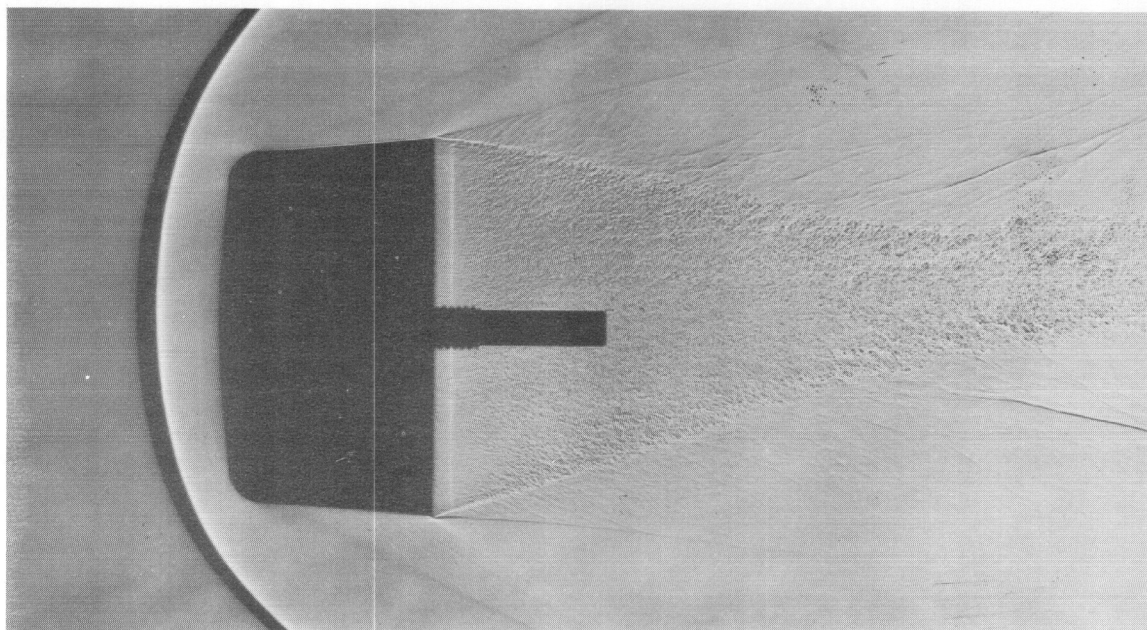
(a) Transition near or behind base; $M_\infty = 3.2$, $R_\infty = 3.0 \times 10^6$.
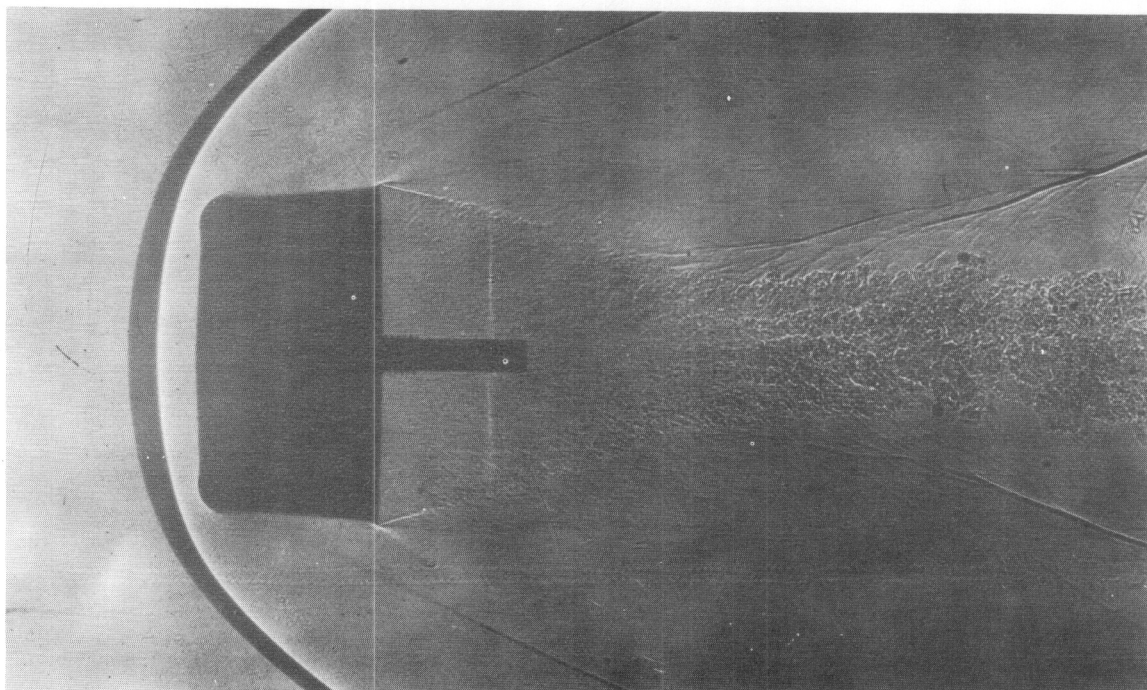
(b) Transition near base; $M_\infty = 3.4$, $R_\infty = 3.2 \times 10^6$.

Figure 7.- Laminar flow on face of model F.
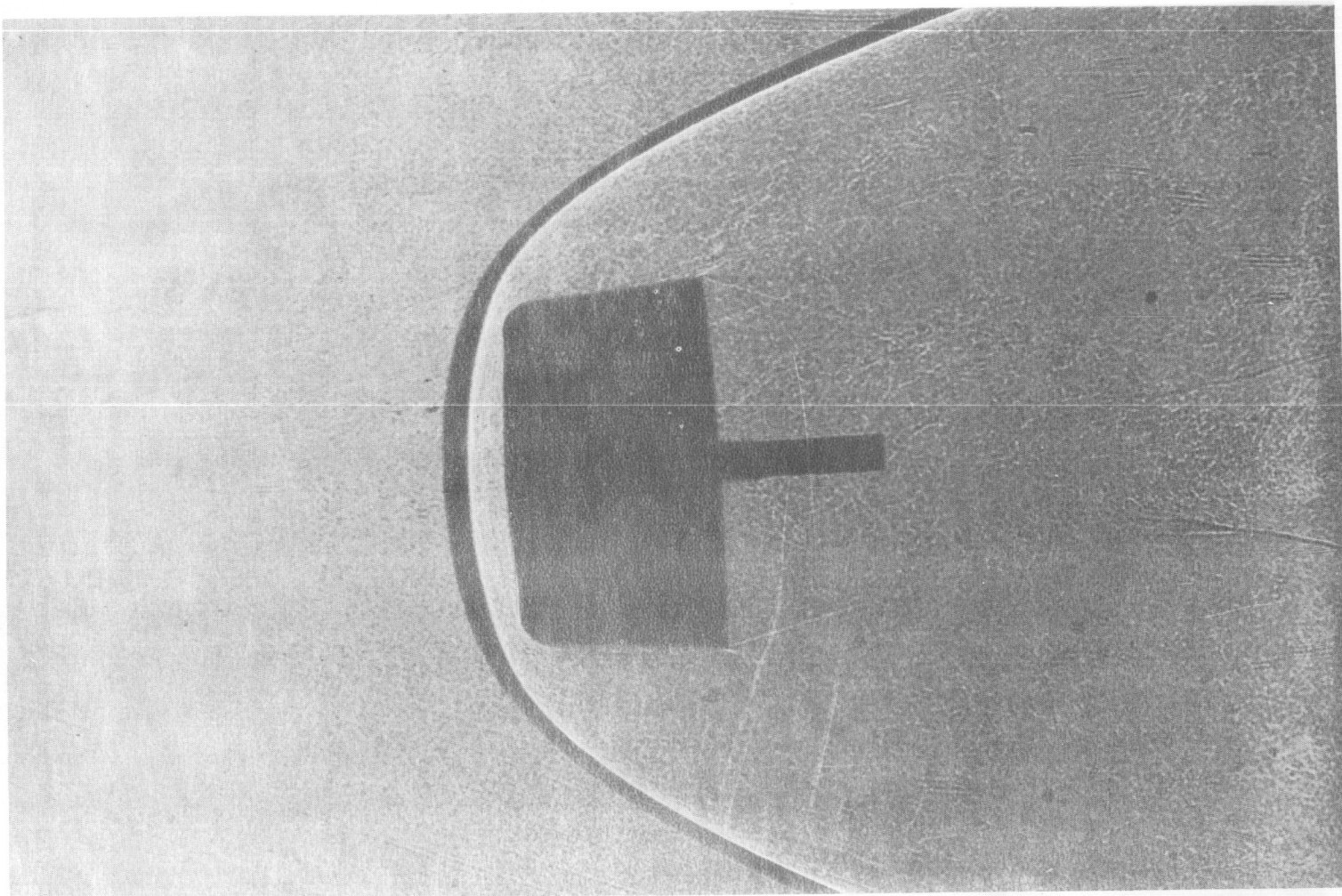
(c) Transition well behind base; $M_\infty = 8.7$, $R_\infty = 4.8 \times 10^6$.

Figure 7.- Concluded.
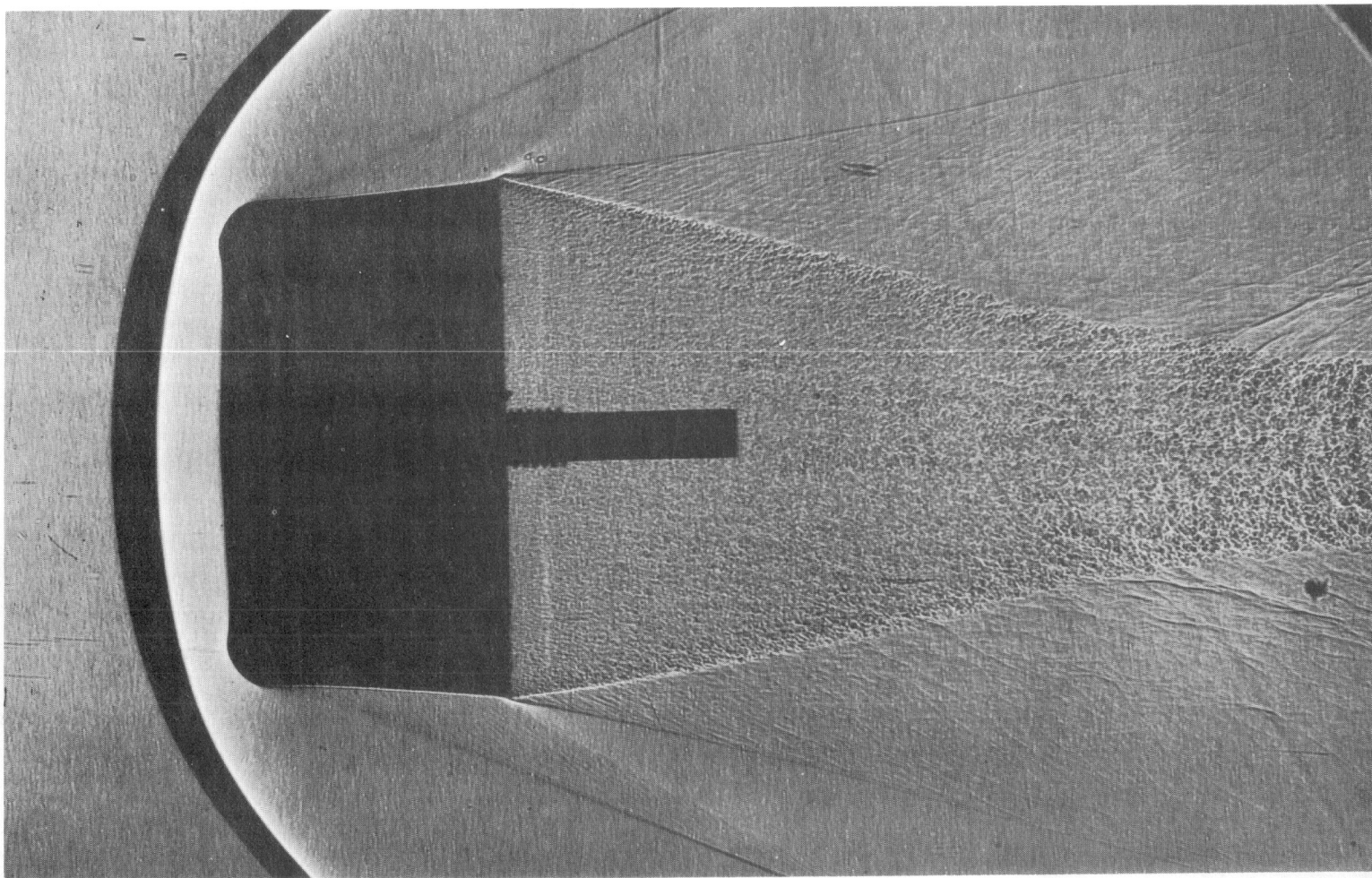
Figure 8.- Laminar flow on face of model F, with transition well forward on sides; $M_\infty = 3.2$, $R_\infty = 9.1 \times 10^6$.
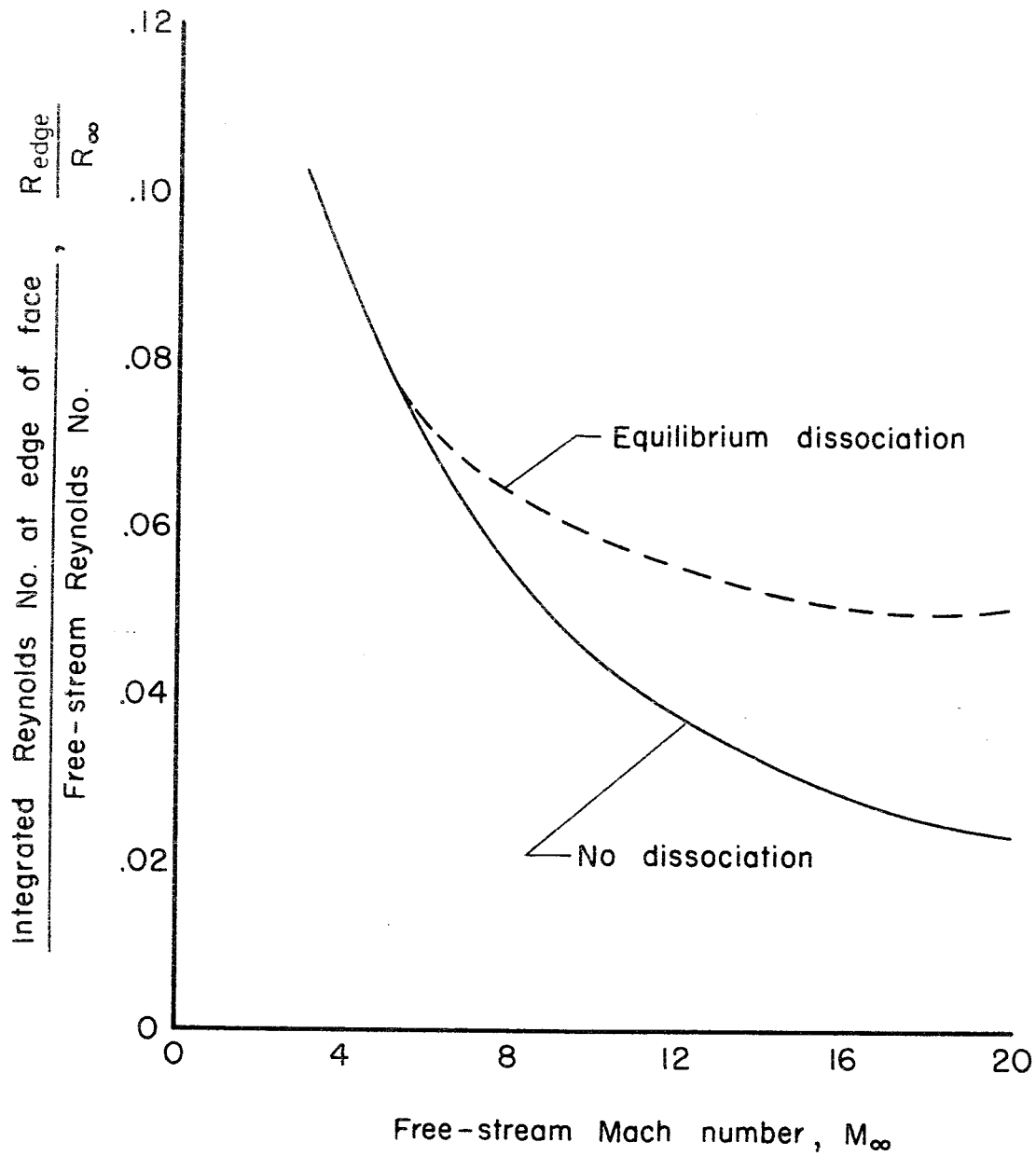
Figure 9.- Variation with Mach number of the ratio of integrated Reynolds number at edge of flat face to free-stream Reynolds number.
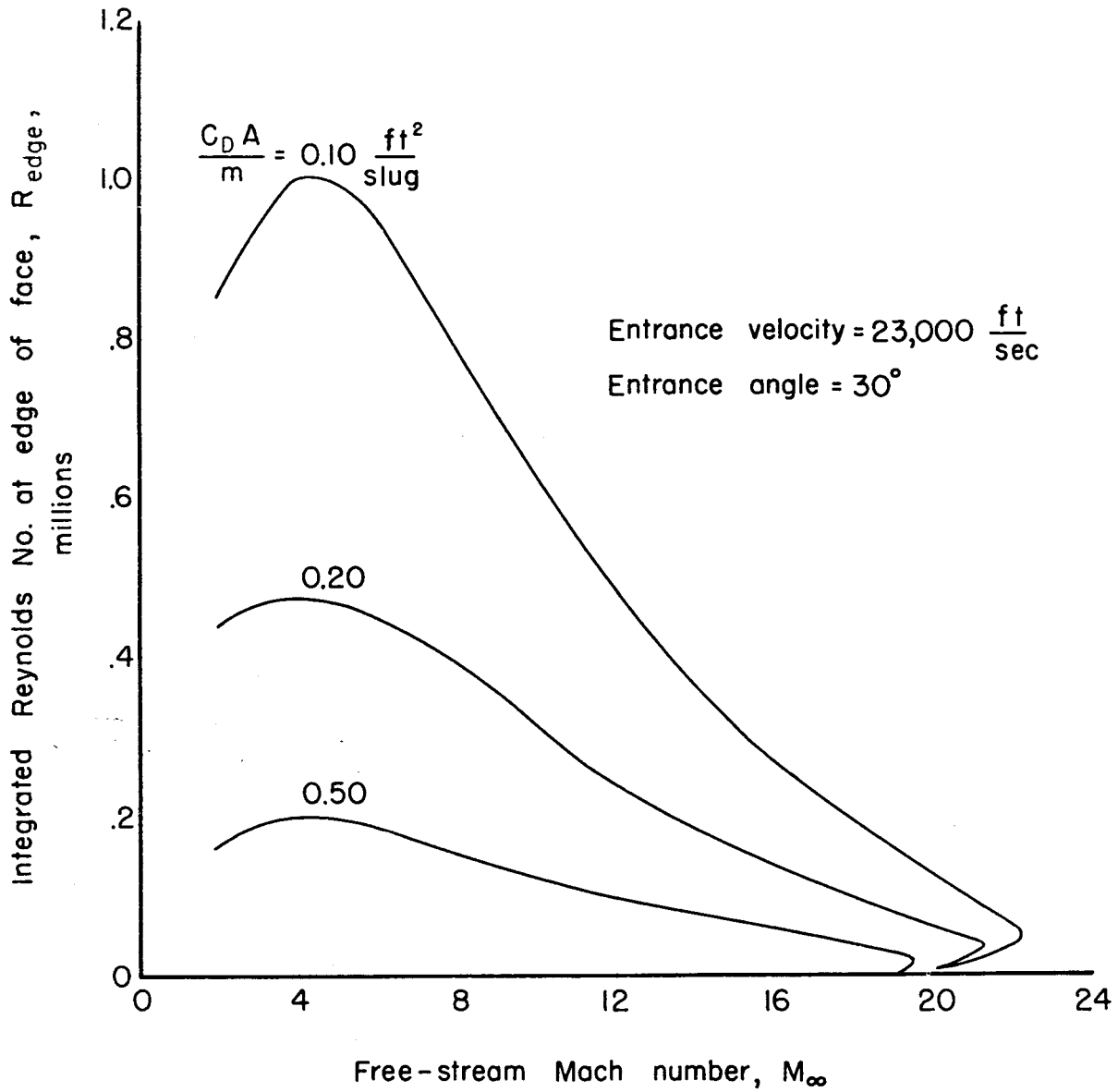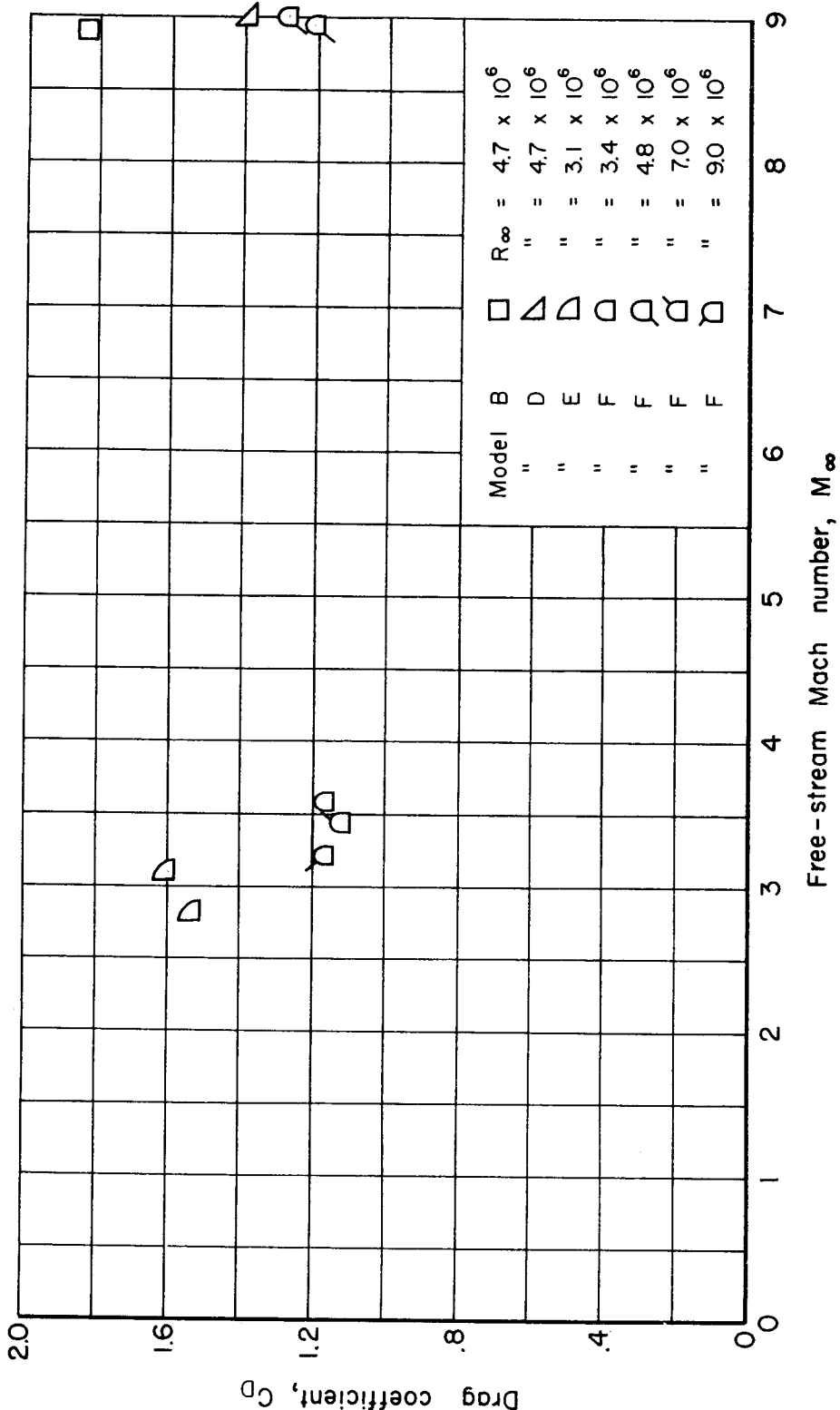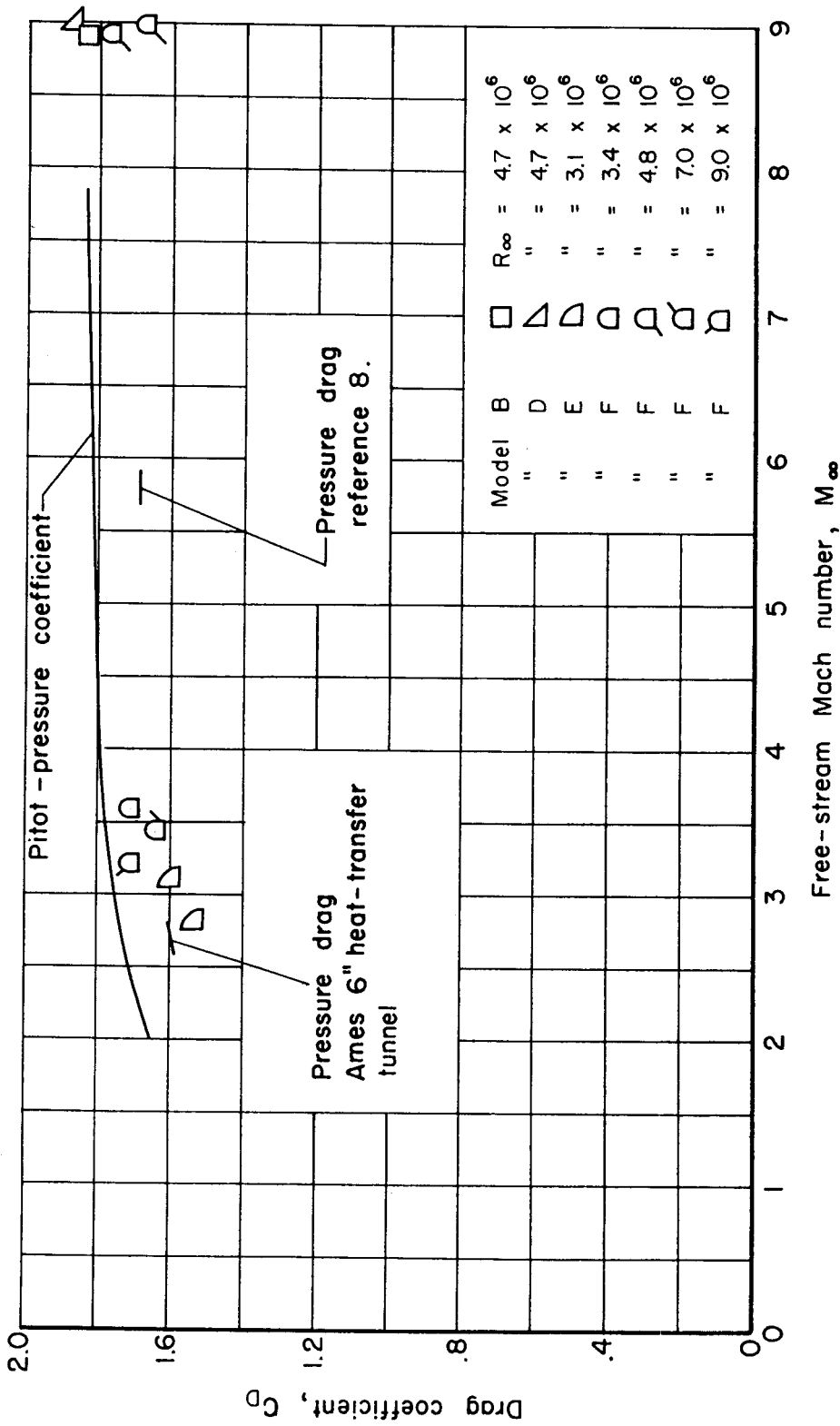
Figure 10.- Variation with Mach number of integrated Reynolds number at edge of 1-foot-diameter flat-faced missile entering the earth's atmosphere. (Case of no dissociation.)

(a) Based on frontal area.

Figure 11.- Drag coefficients.
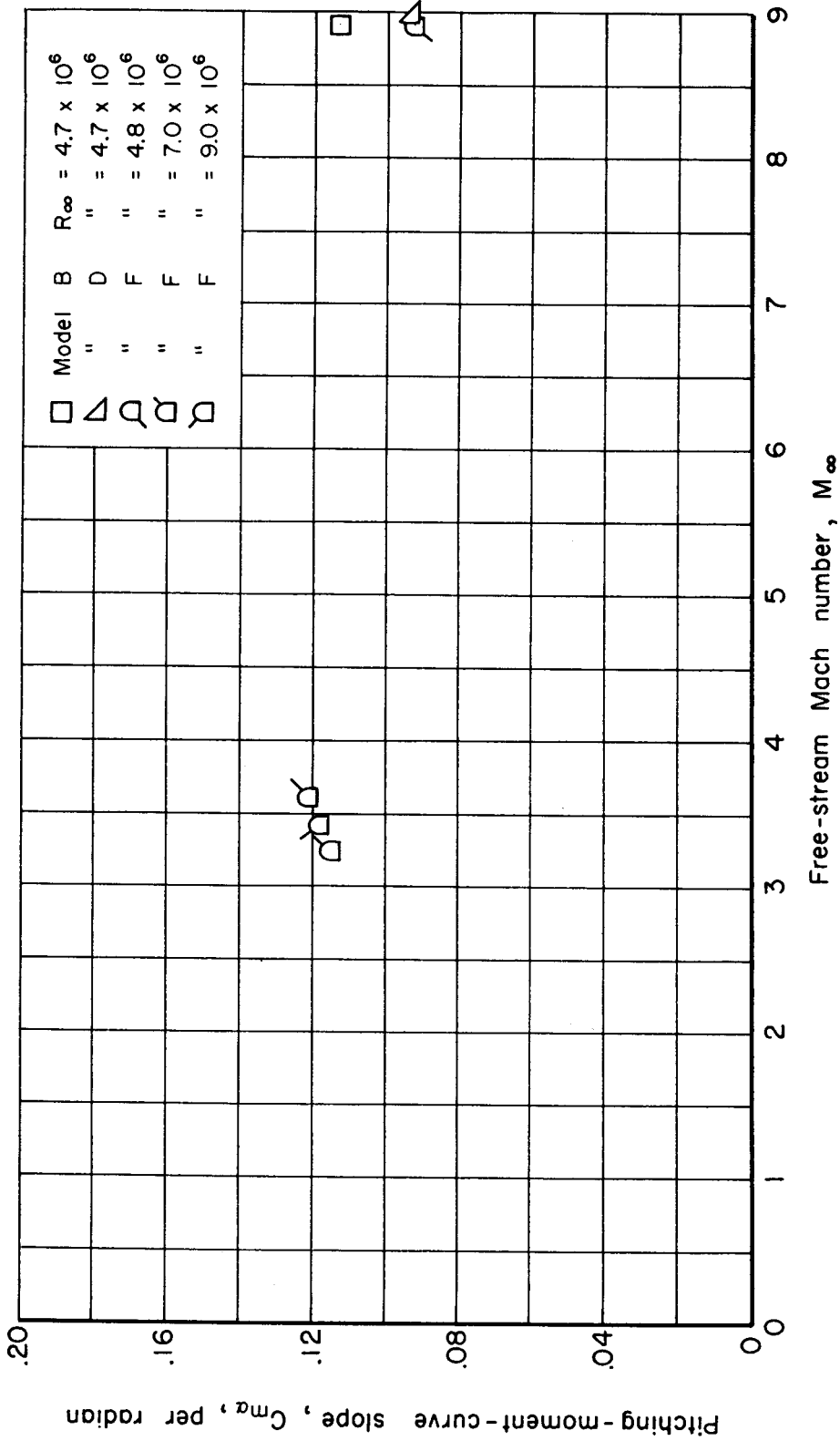
(b) Based on face area.

Figure 11.- Concluded.

Figure 12.— Pitching-moment-curve slopes about center of volume.